

## A global study of GPP focusing on light-use efficiency in a random forest regression model

SUHUA WEI,<sup>1,2</sup> CHUIXIANG YI,<sup>1,2,†</sup> WEI FANG,<sup>1</sup> AND GEORGE HENDREY<sup>1,2</sup>

<sup>1</sup>*School of Earth and Environmental Sciences, Queens College, City University of New York, 65-30 Kissena Boulevard, Flushing, New York 11367 USA*

<sup>2</sup>*The Graduate Center, City University of New York, New York, New York 10016 USA*

**Citation:** Wei, S., C. Yi, W. Fang, and G. Hendrey. 2017. A global study of GPP focusing on light-use efficiency in a random forest regression model. *Ecosphere* 8(5):e01724. 10.1002/ecs2.1724

**Abstract.** Light-use efficiency (LUE) is at the core of mechanistic modeling of global gross primary production (GPP). However, most LUE estimates in global models are satellite based and coarsely measured with emphasis on environmental variables. Others are from eddy covariance towers with much greater spatial and temporal data quality and emphasis on mechanistic processes, but in a limited number of sites. In this study, we conducted a comprehensive global study of tower-based LUE from 237 FLUXNET towers, and scaled up LUEs from in situ tower level to global biome level. We integrated the tower-based LUE estimates with key environmental and biological variables at  $0.5^\circ \times 0.5^\circ$  grid-cell resolutions, using a random forest regression (RFR) approach. Then, we developed a RFR-LUE-GPP model using the grid-cell LUE data. In order to calibrate the LUE model, we developed a data-driven RFR-GPP model using RFR method only. Our results showed LUE varies largely with latitude. We estimated a global area-weighted average of LUE at  $1.23 \pm 0.03 \text{ g C}\cdot\text{m}^{-2}\cdot\text{MJ}^{-1}$  APAR, which led to an estimate of global GPP of  $107.5 \pm 2.5 \text{ Gt C/yr}$  from 2001 to 2005. Large uncertainties existed in GPP estimations over sparsely vegetated areas covered by savannas and woody savannas at middle to low latitude (i.e.,  $20^\circ \text{ S}$ – $40^\circ \text{ S}$  and  $5^\circ \text{ N}$ – $40^\circ \text{ N}$ ) due to the lack of available data. Model results were improved by incorporating Köppen climate types to represent climate/meteorological information in machine-learning modeling. This brought a new understanding to the recognized problem of climate dependence of spring onset of photosynthesis and the challenges in accurately modeling the biome GPP of evergreen broadleaf forests (EBF). The divergent responses of GPP to temperature and precipitation at middle to high latitudes and at middle to low latitudes echo the necessity of modeling GPP separately by latitudes.

**Key words:** biome; enhanced vegetation index (EVI); FLUXNET; gross primary production (GPP); light-use efficiency (LUE); photosynthetically active radiation (PAR); precipitation; random forest regression (RFR); temperature.

**Received** 4 August 2016; revised 1 January 2017; accepted 5 January 2017. Corresponding Editor: Debra P. C. Peters.

**Copyright:** © 2017 Wei et al. This is an open access article under the terms of the Creative Commons Attribution License, which permits use, distribution and reproduction in any medium, provided the original work is properly cited.

† **E-mail:** cyi@qc.cuny.edu

### INTRODUCTION

The terrestrial biosphere is a photosynthetic engine that converts sunlight into biochemical energy that can be later released to sustain living organisms. However, the working efficiency of the photosynthetic engine (i.e., light-use efficiency, LUE) can be affected by changes in climate including temperature, water availability, and

atmospheric  $\text{CO}_2$  concentration. It is well understood that global climate is changing and this may have consequences for terrestrial biosphere gross primary production (GPP) through several mechanisms, including altered LUE, with a potential for triggering positive feedbacks on the rate of climate change (Cox et al. 2000, 2013, Yi et al. 2014, 2015). Spatial and temporal dynamics of biome LUE are key variables for understanding

the relationship between climate drivers and global GPP.

Photons absorbed by a leaf have three possible fates: translation through various paths into heat energy, re-emitted as fluorescence, or converted to chemical energy with LUE of photosynthesis typically in the range of 2–10% of photosynthetically active radiation (PAR). Light-use efficiency is well understood at leaf level, defined as the slope of photosynthesis curve in the light-limited section (Lambers et al. 1998, Medlyn 1998). The leaf photosynthesis curve for a single leaf becomes nonlinear when the chloroplasts are light-saturated. Monteith (1972) proposed the original LUE thermodynamic model for well-watered and fertilized crop plants. At a single leaf level, enzyme kinetic photosynthesis models, such as Farquhar-von Caemmerer-Berry model (Farquhar et al. 1980), provide a quantitative base for understanding how photosynthetic processes are regulated by biotic and abiotic factors, such as atmospheric CO<sub>2</sub> level, water availability, nutrient supply, temperature, and other factors. At canopy level, LUE models ignore these biochemical details and GPP is simply calculated as a product of the fraction of PAR being absorbed by the plant canopy ( $f_{\text{PAR}}$ ) and the LUE ( $\epsilon$ ).

The initial LUE model assumes that all canopy leaves, characterized by leaf area index (LAI), have the same photosynthesis light curve and that CO<sub>2</sub> concentration is uniform through the canopy, that is, “big-leaf model.” In principle, this big-leaf model is constrained by the energy conservation law; that is, plants convert the absorbed light energy into biochemical energy stored in biomass. The simplicity of the LUE or big-leaf model has enabled ecologists to use remote-sensing techniques to estimate global GPP (Field 1991, Prince 1991, Sellers et al. 1996, Goetz et al. 1999, Turner et al. 2003a, b). The absorbed solar energy ( $\text{PAR} \times f_{\text{PAR}}$ ) can be calculated by satellite-derived spectral indices of vegetation, such as normalized difference vegetation index, LAI, and enhanced vegetation index (EVI). The accuracy and resolution of global remote-sensing products of these spectral vegetation indices and  $f_{\text{PAR}}$  have been greatly improved by a few generations of satellite sensors, from the advanced very high-resolution radiometer sensor to the moderate-resolution imaging spectroradiometer (MODIS) sensor (Zhao and Running 2006).

However, most of the uncertainty in global-scale GPP estimation by LUE models is associated with determination of LUE ( $\epsilon$ ) itself. This could be improved if we were able to assess the influences of spatial and temporal variations in environmental factors (temperature, soil moisture, water stress, nutrient availability) that impact LUE with remote-sensed spectral vegetation indices and reflectance at a larger or global scale (Hilker et al. 2008). For example, the MODIS17 algorithm is calculated as:

$$\text{GPP} = \text{PAR} \times f_{\text{PAR}} \times \epsilon \quad (1)$$

$\epsilon$  uses a look-up table containing biome-specific information about the maximum LUE  $\epsilon_{\text{max}}$ , daily minimum temperature ( $T_{\text{min}}$ ), and vapor pressure deficit ( $D$ ) of each biome type. The  $\epsilon_{\text{max}}$  is adjusted to account for the limiting effects of climatic variables on  $\epsilon$  (Running et al. 2004):

$$\epsilon = \epsilon_{\text{max}} \times T_{\text{min}} \times D. \quad (2)$$

The eddy covariance (EC) technique provides ground-truth measurements for calibration of remote-sensing LUE models at tower-footprint scale ( $\sim\text{km}^2$ ). The EC measurements include net ecosystem exchanges (NEE) of carbon dioxide, water vapor, and energy, as well as environmental conditions. Attributes of EC data that can contribute most to remote-sensing LUE models include the following: (1) NEE data represent a whole-ecosystem estimate of carbon exchange (including both aboveground and belowground) with the atmosphere at tower-footprint scale; (2) additional abiotic variables that control NEE are measured at a EC-tower sites (temperature, precipitation, vapor pressure deficit, net radiation, PAR, albedo, soil moisture, wind speed, and direction etc.); (3) the temporal dimension of data is continuous from hours to years; and (4) measurements are collected from “natural” conditions with minimal disturbances (Baldocchi et al. 2001).

Net ecosystem exchanges data are not perfect, having significant errors when air is strongly stratified over complex terrain during calm nighttime (Goulden et al. 1996, Yi et al. 2000, 2008, Massman and Lee 2002, Aubinet et al. 2003, Feigenwinter et al. 2005, 2008, 2010a, b, Aubinet 2008, Finnigan 2008, Montagnani et al. 2009). Gross primary production data used by LUE modelers are derived from daytime NEE data under well-mixed conditions. Although daytime GPP data are indirectly

associated with nighttime errors through terrestrial respiration estimation (Yi et al. 2004), tower-based GPP data are more defensible (Baldocchi 2008), offering a unique opportunity to examine LUE for a whole natural ecosystem at tower-footprint scale (Ruimy et al. 1995).

Although significant progress in estimating satellite-based GPP has been achieved, uncertainties still exist among GPP models (Raczka et al. 2013, Yuan et al. 2014). Evaluation of average GPP from 26 models using satellite data against estimated GPP at 39 EC flux towers across United States and Canada found the LUE models usually overestimate GPP in the spring, fall, and winter, and underestimate GPP in the summer. Light-use efficiency models over-predicted GPP for dry conditions and for temperatures below 0°C (Schaefer et al. 2012). The poor predictabilities of these models could be caused by (1) the spatial and temporal dynamics of LUE which were not adequately represented, or (2) the assumption of uniform linear constraints of water stress and temperature stress over various biomes which could be unrealistic. To avoid these problems, other researchers tried complementary data-oriented modeling or diagnostic modeling in which general relationship between existing data was first inferred at the site level and then applied to large scale using grids of explanatory variables. Pure data-driven models, particularly those applying machine-learning methods (e.g., artificial neural networks, support vector machine, or random forest regression [RFR]), are increasing in utility and are considered as benchmarks for LUE models (Beer et al. 2010).

In this research, we conducted a comprehensive analysis of LUE across a wide variety of vegetation. To do this, we integrated a large number of in situ measurements from 237 FLUXNET EC towers in order to study the spatiotemporal patterns of LUE determined at EC-tower scale. The goal of this paper was to translate these tower-scale LUE estimates into global scale of remote sensing.

We designed two algorithms applying different LUE schemes in modeling global GPP. One scales up LUEs with a RFR approach (RFR-LUE-GPP). The other was derived as a data-driven benchmark model using a RFR method (RFR-GPP), with no specific assumptions or any in situ LUE data training. The model outputs were validated against FLUXNET-referenced GPP data.

## METHODS

### *Land products*

*Fraction of absorbed PAR.*—Monthly  $f_{\text{PAR}}$  product was generated from an analysis of Sea-viewing Wide Field-of-view Sensor (SeaWiFS) data with  $0.5^\circ \times 0.5^\circ$  spatial resolution obtained from the Institute for Environment and Sustainability at the Joint Research Center of the European Commission. The quality of this dataset was assessed and validated (Gobron et al. 2006).

*Enhanced vegetation index.*—The EVI data were obtained from the MODIS MOD13C2 product, provided by NASA Land Processes Distributed Active Archive Center (LP DAAC), USGS/Earth Resources Observation and Science (EROS) Center, Sioux Falls, South Dakota, USA. We used monthly L3 global with  $0.05^\circ$  resolution. This dataset was resampled to a spatial resolution of  $0.5^\circ \times 0.5^\circ$  with nearest neighbor interpolation, which was processed in the SciPy module of Python (Python Software Foundation, <https://www.python.org/>). All spatial interpolations mentioned in this paper follow this procedure.

*Plant function type.*—The land cover information, or plant function type, was determined by MODIS land cover product MOD12Q1, provided by NASA Land Processes Distributed Active Archive Center (LP DAAC), USGS/Earth Resources Observation and Science (EROS) Center, Sioux Falls, South Dakota, USA. The land cover types were classified using the IGBP global vegetation classification scheme. The spatial resolution of the dataset was  $0.5^\circ \times 0.5^\circ$ : <http://glcf.umd.edu/data/lc/>.

### *Meteorological data*

*Shortwave incoming radiation.*—The monthly net shortwave radiation data (January 2001–December 2005) were obtained from the National Centers for Environmental Prediction (NCEP). The radiation reanalysis data were originally at a spatial resolution of  $1.895^\circ \times 1.915^\circ$ . We resampled this dataset into  $0.5^\circ \times 0.5^\circ$  with nearest neighbor interpolation.

*Temperature.*—The monthly temperature data (January 2001–December 2005) were obtained by surface reanalysis data of NCEP ( $0.5^\circ \times 0.5^\circ$  spatial resolution), obtained from the website file <http://www.esrl.noaa.gov/psd/data/gridded/data.ncep.reanalysis.derived.pressure.html>.

Table 1. Biome classifications sampled at FLUXNET sites with number of sites ( $n_{\text{site}}$ ) and their abbreviations.

Biome	Description	$n_{\text{site}}$
CRO	Croplands	30
CSH	Closed shrublands	6
DBF	Deciduous broadleaf forests	31
EBF	Evergreen broadleaf forests	16
ENF	Evergreen needleleaf forests	65
GRA	Grasslands	42
MF	Mixed forests	11
OSH	Open shrublands	12
SAV	Savannas	2
WET	Permanent wetlands	15
WSA	Woody savannas	7

*Precipitation.*—The monthly precipitation data were obtained from NOAA's Precipitation Reconstruction over Land ( $0.5^\circ \times 0.5^\circ$  spatial resolution). The global analyses were defined by interpolation of gauge observations over land and by reconstruction of historical observations over the ocean. More details about this dataset are in Chen et al. (2002) and <http://www.esrl.noaa.gov/psd/data/gridded/data.precl.html>.

*FLUXNET data.*—Flux data were obtained from the FLUXNET-La Thuile database, in the half-hourly flux and meteorological data from AmeriFlux, FLUXNET-Canada, Carbon Europe IP, USCCC, China Flux, OZFLux, Carbon Africa, and Asia Flux networks, and were compiled. The latitudes of FLUXNET sites range from  $71^\circ$  N to  $37^\circ$  S, covering polar tundra, maritime temperate, continental temperate, humid subtropical, Mediterranean, arid, semi-arid, tropical monsoon, and tropical wet-and-dry climates. These data were quality-controlled and gap-filled with consistent methods (Papale et al. 2006). Gross primary production data were derived from NEE data with a nonlinear regression algorithm (Reichstein et al. 2005). The biome classification and numbers of sites per biome are described in Table 1.

*Köppen-Geiger climate classifications (Kp).*—Peel et al. (2007) updated a global map of climate using the Köppen-Geiger system based on a large global data set of long-term monthly precipitation and temperature station time series. Under the Köppen-Geiger classification scheme, climate zones were grouped as follows: Group A, tropical; Group B, dry (arid and semi-arid); Group C, temperate; Group D, continental; and

Group E, polar and alpine. Specific climate classifications are described in Appendix S1: Table S1. The Köppen-Geiger climate classifications are illustrated in Fig. 1.

#### Calculation of light-use efficiency from FLUXNET tower sites

Light-use efficiency is defined as the number of moles of carbon fixed per mole incident light and declines with increasing light intensity (PPFD, or  $Q$ ) as the photosynthetic light response curve saturates (Ruimy et al. 1995, Barton and North 2001). The response of  $\text{CO}_2$  flux between the ecosystem and the atmosphere to  $Q$  (the light response curve) can be described by a rectangular hyperbola model (Ruimy et al. 1995, Falge et al. 2001, Yi et al. 2004, Xiao 2006, Wei et al. 2014):

$$\text{NEE} = R_e - \frac{\varepsilon Q A_{\text{max}}}{\varepsilon Q + A_{\text{max}}}. \quad (3)$$

NEE is the net ecosystem exchange directly measured from FLUXNET.  $A_{\text{max}}$  is photosynthetic capacity.  $\varepsilon$  is LUE (or apparent quantum yield), representing the initial slope of the light response curve.  $R_e$  is ecosystem dark respiration. This model has been used in a number of past studies to analyze the response of NEE to light intensity, and to partition NEE into its component processes (Ruimy et al. 1995, Falge et al. 2001, Xiao 2006).

We aggregated half-hourly measured PPFD and NEE data to monthly scale. MATLAB (The MathWorks Inc., Natick, Massachusetts, USA) curve fitting toolbox was used to fit the data to the first model (3), following the constraints:  $0 < \varepsilon < 10$  ( $\text{g C} \cdot \text{m}^{-2} \cdot \text{MJ}^{-1}$  APAR),  $0 < A_{\text{max}} < 100$   $\mu \text{mol} \cdot \text{m}^{-2} \cdot \text{s}^{-1}$ , and  $R_e > 0$ . We compared the model performances based on their goodness-of-fit coefficient  $r^2$ . The datasets with  $r^2 < 0.4$  were arbitrarily discarded (Ruimy et al. 1995).

#### Scale up LUE to global scale—Experimental design

Machine-learning approaches were employed in which results were less contingent on complex combinations of scientific assumptions. Upscaling of EC carbon fluxes with machine-learning method to large regions was conducted for the North America (Yang et al. 2007, Xiao et al. 2014), Europe (Papale and Valentini 2003, Vetter et al. 2008, Jung et al. 2009), and the globe (Jung

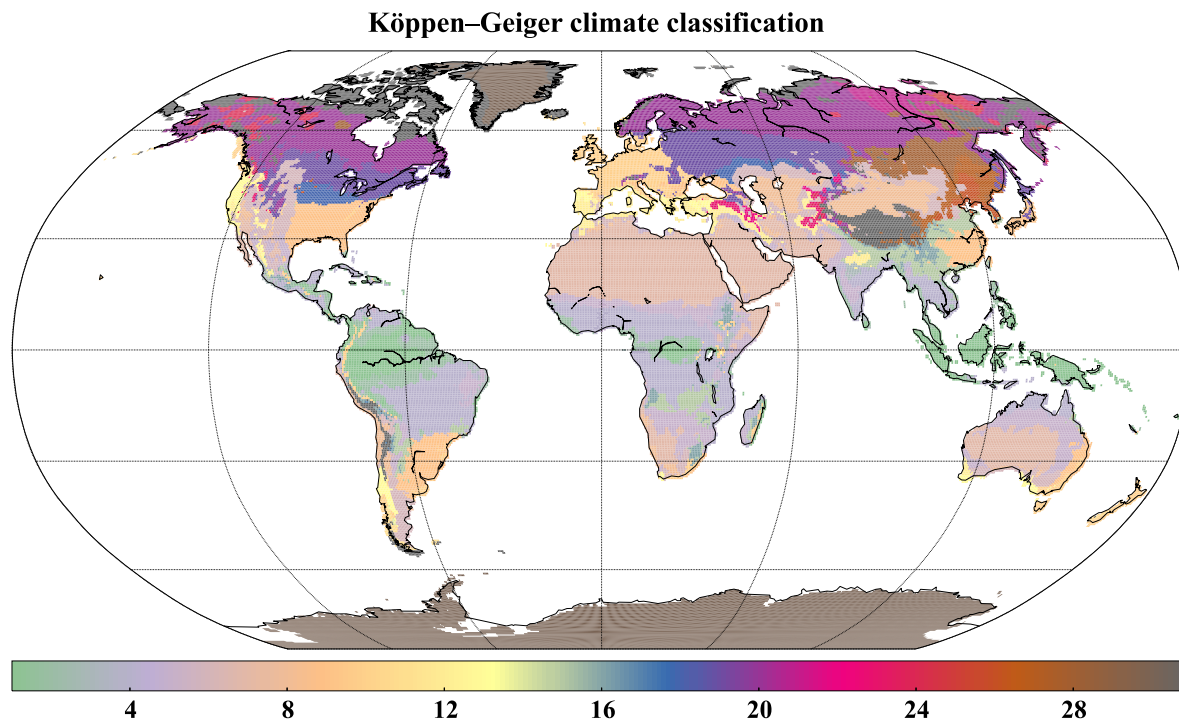


Fig. 1. Köppen–Geiger climate classifications. Climate types are color-coded on the map as follows: 1: Af; 2: Am; 3: As; 4: Aw; 5: BSh; 6: BSk; 7: BWh; 8: BWk; 9: Cfa; 10: Cfb; 11: Cfc; 12: Csa; 13: Csb; 14: Csc; 15: Cwa; 16: Cwb; 17: Cwc; 18: Dfa; 19: Dfb; 20: Dfc; 21: Dfd; 22: Dsa; 23: Dsb; 24: Dsc; 25: Dsd; 26: Dwa; 27: Dwb; 28: Dwc; 29: Dwd; 30: EF; 31: ET. Köppen climate symbols are described in Appendix S1: Table S1.

et al. 2011) at various temporal scales. However, being essentially statistical approaches, the data-oriented models were dependent on the availability of sufficient data (Beer et al. 2010). In addition, data-oriented models, so far, have provided little insights on the fundamental physical mechanisms of biosphere–atmospheric carbon exchanges.

To take advantages of these approaches, and to bridge the knowledge gap of model uncertainties generated by both model structures, we design one LUE algorithm and one diagnostic model to estimate global GPP in this study: (1) RFR-LUE-GPP model using upscaled LUE data by the RFR method and (2) RFR-GPP model (diagnostic model): pure data-driven method by RFR.

*The RFR-LUE-GPP model.*—In this half-process LUE model, detailed information from LUE datasets calculated in (3) was translated from tower-footprint scale into remote-sensing scale. The general relationships between LUE and explanatory data were first trained at site level, and then applied globally by using global grids

of explanatory variables as described in the following equation:

$$\varepsilon_{\text{grid}} = f_{\text{RFR}}(\text{EVI}, f_{\text{PAR}}, \text{temperature}, \text{precipitation}, \text{incoming shortwave radiation}, \text{Köppen climate types}, \text{biome types}). \quad (4)$$

Eq. 4 represents the training method of the RFR, a machine-learning algorithm for a predictive model, in which each tree in the ensemble is built from a sample drawn with replacement (i.e., a bootstrap sample) from the training set. In addition, when splitting a node during the construction of the tree, the split that is chosen is no longer the best split among all features. Instead, the split that is picked is the best split among a random subset of the features. As a result of this randomness, the bias of the forest usually increases slightly (with respect to the bias of a single non-random tree) but, due to averaging, its variance also decreases, usually more than compensating for the increase in bias, hence yielding an overall

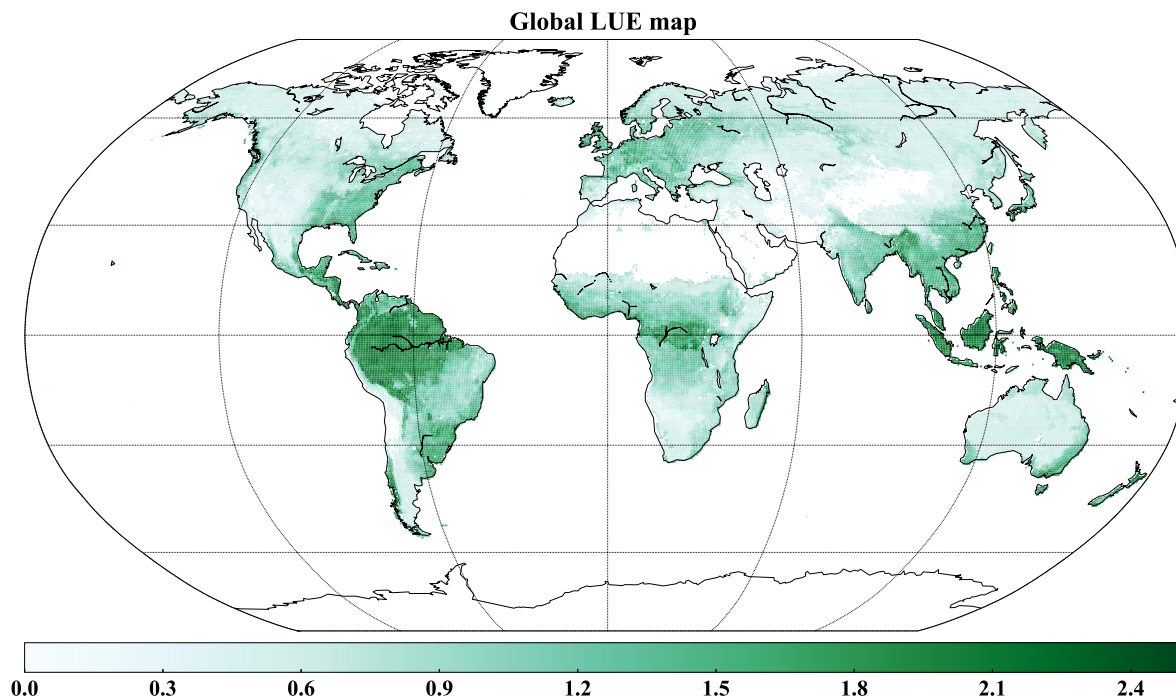


Fig. 2. Global light-use efficiency (LUE) map ( $\text{g C}\cdot\text{m}^{-2}\cdot\text{MJ}^{-1}$  APAR). A global area-weighted average of  $1.23 \pm 0.03 \text{ g C}\cdot\text{m}^{-2}\cdot\text{MJ}^{-1}$  APAR was derived by scaling up tower-based LUE to the globe with random forest regression method. Light-use efficiency displaying large seasonal variations is shown in Appendix S1: Fig. S1.

better model. We use Python scikit-learn module for this analysis (Pedregosa et al. 2011).

The training performance of  $\varepsilon_{\text{grid}}$  was evaluated based on a fivefold cross-validation in which data were divided into five equal subsets. The target values were selected as one of the five subsets. The target values were predicted based on the training on the remaining four subsets. This process was repeatedly looped through all subsets, and the GPP was calculated as:

$$\text{GPP} = \text{PAR} \times f_{\text{PAR}} \times \varepsilon_{\text{grid}}. \quad (5)$$

*The RFR-GPP model.*—In this diagnostic model, we only applied the RFR to train the data from FLUXNET sites and to scaling up to the globe.

$$\text{GPP} = f_{\text{RFR}}(\text{EVI}, f_{\text{PAR}}, \text{temperature}, \text{precipitation}, \text{incoming shortwave radiation}, \text{Köppen climate types}, \text{biome types}). \quad (6)$$

The modeling performances were also evaluated based on fivefold cross-validation as discussed above.

## RESULTS

### Prediction of LUE at the global scale

A global area-weighted annual average of LUE at  $1.23 \pm 0.03 \text{ g C}\cdot\text{m}^{-2}\cdot\text{MJ}^{-1}$  APAR was derived by scaling up tower-based LUE to the globe with RFR method (Fig. 2). Light-use efficiency varies largely in spatial domain and temporal domain (Appendix S1: Fig. S1). In central Africa around the Democratic Republic of Congo (Köppen Af), where areas are covered by evergreen broadleaf forests (EBF), LUE values remained high for the entire year. In the southern part of Africa ( $15^\circ \text{ S}$  to  $\sim 35^\circ \text{ S}$ ), the major vegetation types were closed and open shrublands (OSH) under arid climate (Köppen BWh and BWk), and photosynthesis was inhibited by lack of moisture, resulting in low LUE for all year. There were mosaic vegetation and cropland along the western coastal line, displaying high LUE during growing seasons in the Southern Hemisphere (December–February).

In North America, photosynthesis of boreal ecosystems was turned off during cold winter months, but recovered in April (Köppen C group).

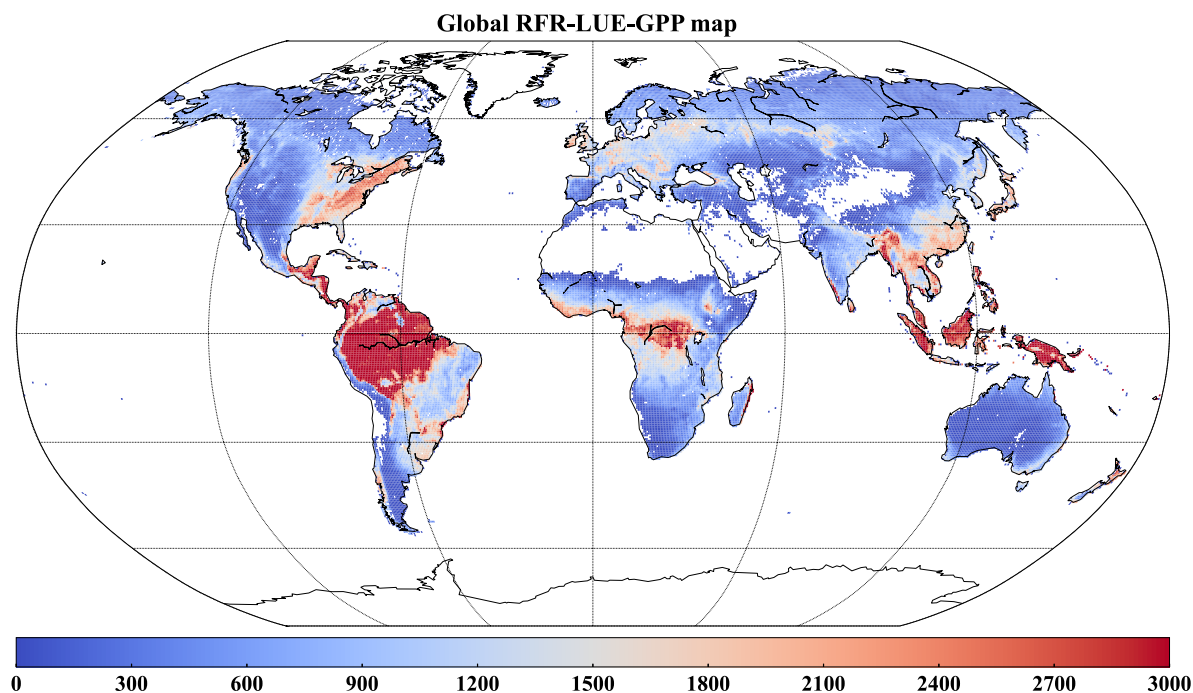


Fig. 3. Mean global GPP map (2001–2005;  $\text{g C}\cdot\text{m}^{-2}\cdot\text{yr}$ ) by RFR-LUE-GPP model. An area-weighted annual mean GPP of  $107.5 \pm 2.5 \text{ Gt C/yr}$  was estimated by this model. GPP, gross primary production; RFR, random forest regression; LUE, light-use efficiency.

During June and July, LUE of some deciduous broadleaf forests (DBF) and mixed forests (MF) areas reached above  $3.0 \text{ g C}\cdot\text{m}^{-2}\cdot\text{MJ}^{-1}$  APAR. The same pattern was also found for DBF and MF in Eurasia at the same latitudes. In South America, most of the areas between  $10^\circ \text{ N}$ – $16^\circ \text{ S}$  and  $50^\circ \text{ W}$ – $78^\circ \text{ W}$  were covered by EBF. Although high LUE values were common all year long in South America, they were particularly high around February and March when it was wet season in the tropical monsoon climate (Köppen Am), and relatively low around September and October in dry season, which was consistent with some studies' finding that carbon sequestration rates were greater for tropical forests during wet season (Goulden et al. 2004).

The northern part of Australia is covered with savanna (SAV), while central Australia is covered with OSH and EBF occur along the southeast coastline. There were only three FLUXNET towers available for Australia. One was a woody savanna (WSA, Köppen Aw) site close to the Equator and the other two were both EBF sites under temperate climate near  $35^\circ \text{ S}$ – $38^\circ \text{ S}$  in the southeast

region. No SAV or OSH sites were available for the model training for Australia and therefore were not represented in the LUE-GPP estimate for this region. As expected, EBF LUE values were relatively high all year long along the southeast coastline. The OSH LUE values were very high in December at central Australia. Since the only OSH similar to Australia OSH is in China Northern Hemisphere (CN-Ku2,  $40.3^\circ \text{ N}$ ,  $108.5^\circ \text{ E}$ ) under Bsk climate, in which the highest LUE happens during June–August, incorporating OSH data from Northern Hemisphere site would further skew the modeling estimate in Australia. The unexpected high values estimated by the global model in central Australia in July and August (Southern Hemisphere) were therefore unrealistic and likely caused by the unbalanced representation of all vegetation types.

#### Prediction of global GPP

Higher global GPP ( $121.5 \pm 3.6 \text{ Gt C/yr}$ ) was predicted by the RFR-GPP model and lower value ( $107.5 \pm 2.5 \text{ Gt C/yr}$ ) by the RFR-LUE-GPP model (Fig. 3). Scatter plots of comparison between

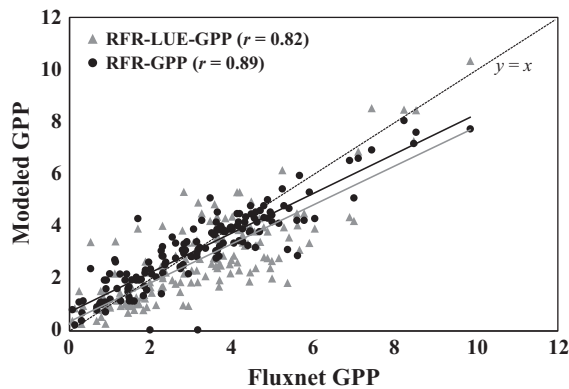


Fig. 4. Scatter plots of comparison between model outputs ( $y$ -axis,  $\text{g C}\cdot\text{m}^{-2}\cdot\text{d}^{-1}$ ) and reference GPP derived by covariance at FLUXNET sites ( $x$ -axis,  $\text{g C}\cdot\text{m}^{-2}\cdot\text{d}^{-1}$ ). Data points were aggregated to annual mean for each site. Benchmark model (RFR-GPP) showed a higher Pearson linear coefficient ( $r = 0.89$ ) than RFR-LUE-GPP model ( $r = 0.82$ ). GPP, gross primary production; RFR, random forest regression; LUE, light-use efficiency.

model outputs and reference GPP derived by covariance at FLUXNET sites are shown in Fig. 4. Data points were aggregated to annual mean for each site. The benchmark model (RFR-GPP) had a

higher Pearson linear coefficient ( $r = 0.89$ ) in contrast to RFR-LUE-GPP ( $r = 0.82$ ). Large differences between tower-LUE-GPP and RFR-LUE-GPP occurred among the middle to low latitude biomes over  $10^{\circ}\text{S}$ – $40^{\circ}\text{S}$  and  $5^{\circ}\text{N}$ – $40^{\circ}\text{N}$  (Fig. 5 gray shadow (a) and (b)) where the differences in WSA, SAV, and WSA dominated. RFR-LUE-GPP model estimated lower GPP at these areas. RFR-GPP estimated OSH GPP at  $11.6\text{ Gt C/yr}$ , which contributed 9.5% to the total GPP. In contrast, RFR-LUE-GPP model estimated  $4.8\text{ Gt C/yr}$ , only accounting for 4.5% of the total GPP (Table 2). Similarly, RFR-GPP estimated higher GPP of SAV and WSA, combined at  $26.8\text{ Pg C/yr}$ , comparing to RFR-LUE-GPP model at  $16.8\text{ Pg C/yr}$  (Table 2). Evergreen broadleaf forests GPP was estimated around  $39.5\text{ Gt C/yr}$  by the RFR-GPP model and  $34.4\text{ Gt C/yr}$  by the RFR-LUE-GPP model (Table 2). Gross primary production of EBF ranked highest among all the ecosystems (Zhao et al. 2005; Beer et al. 2010 and this study). However, poor prediction of EBF GPP in many reported studies has been a great challenge among both LUE-based models of the global terrestrial carbon cycle (Yuan et al. 2014) and data-oriented machine-learning models (Tramontana et al. 2015). Incorporating Kp data to represent climate/meteorological information in machine-learning

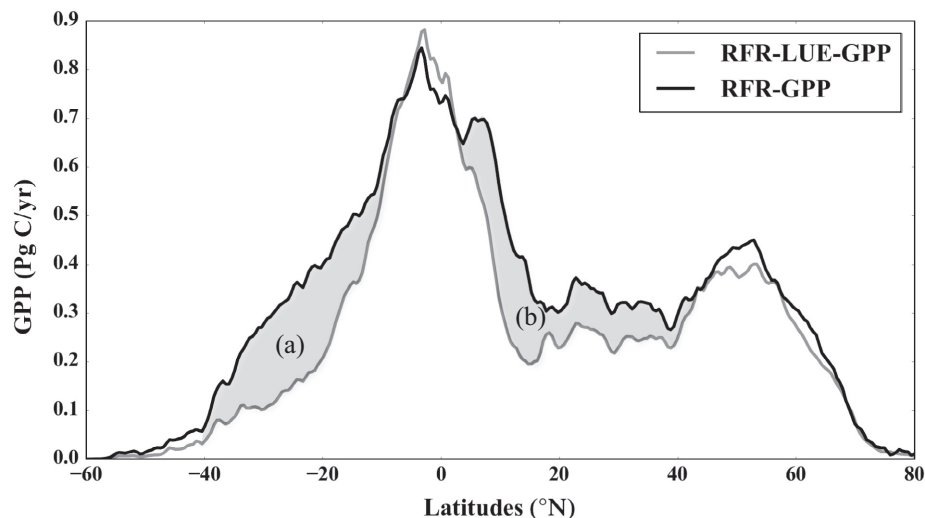


Fig. 5. GPP grid distribution along the latitudes by RFR-LUE-GPP model (gray line) and RFR-GPP model (black line). RFR-GPP estimated much higher GPP of sparsely vegetated areas along middle to low latitudes (gray shade (a) and (b)) due to higher estimated GPP of open shrublands (OSH), WSA and savannas (SAV). GPP, gross primary production; RFR, random forest regression; LUE, light-use efficiency.

Table 2. Total GPP of different biomes in two models.

Modeled GPP	ENF	EBF	DBF	MF	CSH	OSH	WSA	SAV	GRA	WET	CRO	Tundra	Total (Pg C/yr)
RFR-LUE-GPP	2.0	39.5	2.56	10.8	0.03	4.8	12.0	9.8	6.1	0.5	15.4	2.7	107.5
RFR-GPP	2.2	34.4	2.36	9.8	0.08	11.6	15.7	15.2	9.9	0.5	18.1	1.6	121.5

Note: GPP, gross primary production; RFR, random forest regression; LUE, light-use efficiency; CSH, closed shrublands; DBF, deciduous broadleaf forests; EBF, evergreen broadleaf forests; GRA, grasslands; MF, mixed forests; SAV, savanna; WET, permanent wetlands; ENF, evergreen needleleaf forests.

modeling achieved good modeling performance in predicting tropical EBF GPP:  $r = 0.83$  in RFR-GPP and  $r = 0.81$  in RFR-LUE-GPP (Appendix S1: Fig. S2, sites  $n = 9$ ). Reasons for EBF GPP uncertainties are discussed in the Discussion section. Our results indicated the effects of biome type and seasonality and their interaction on LUE were highly significant ( $***P < 0.001$ , Table 3). Aggregated to biome level, LUE of vegetation at middle to high latitudes displayed an evident temporal pattern with one main peak in the summer months as anticipated (Figs. 6, 7), while vegetation at lower latitude depended highly on individual sites and no apparent temporal trend was found (Fig. 8). Evergreen broadleaf forests, WSA, and SAV sites were mainly located at middle to low latitude (Fig. 6). In contrast to other biomes, these three vegetation types tended to exhibit less seasonality in LUE (Fig. 8); instead, both SAV sites and EBF sites showed patterns of high LUE values in wet season and low LUE values in dry seasons.

There were two geographically distinct groups of EBF sites in this study (Fig. 8). One group (EBF\_L) consisted of sites from tropical countries

Table 3. A two-factor ANOVA ( $\alpha = 0.05$ ) test was conducted on the biome and seasonality effects on light-use efficiency (LUE).

Source	SS	df	MS	F	P-value	Significant
Biome	226.25	5	45.25	11.65	0.00***	Yes
Months	253.52	11	23.08	5.94	0.00***	Yes
Inter	213.55	55	3.89	3.51	0.00***	Yes
Within	796.45	720	1.11			
Total	1489.78	791	1.89			

Notes: DBF, deciduous broadleaf forests; EBF, evergreen broadleaf forests; GRA, grasslands; MF, mixed forests; ENF, evergreen needleleaf forests. Equal numbers of sites from six major biomes (EBF, DBF, ENF, MF, OSH, and GRA) were randomly chosen for the test ( $n = 11$  for each biome). There were statistically significant effects of biome and seasonality as well as their interaction on LUE ( $***P < 0.001$ ).

including Brazil, French Guyana, Indonesia, and Vanuatu, with the climate of tropical rainforest, tropical monsoon, and tropical savanna. The latitudes of these sites range from  $15.4^\circ$  S– $5.3^\circ$  N. The other group (EBF\_M) covered mid-latitude European countries, such as France, Italy, Portugal (Mediterranean climate) and Australia (oceanic climate). The latitudes range from  $35.6^\circ$  S to  $37.4^\circ$  S in Southern Hemisphere and from  $38.5^\circ$  N to  $43.7^\circ$  N in Northern Hemisphere. Tropical EBF had a monthly LUE of  $2.52 \text{ g C} \pm 0.3 \text{ m}^{-2} \cdot \text{MJ}^{-1}$  APAR ( $n = 9$ ), while mid-latitude EBF only had a monthly LUE of  $1.82 \pm 0.26 \text{ g C} \cdot \text{m}^{-2} \cdot \text{MJ}^{-1}$  APAR on average ( $n = 7$ ). Two-way ANOVA test on the effects of latitude and seasonality on EBF LUE showed that tropical EBF LUE values were significantly higher than mid-latitude EBF LUE values ( $**P < 0.01$ , Table 4). The effect of seasonality and its interaction with latitude on LUE of EBF was not statistically significant ( $P > 0.05$  for both, Table 4).

Deciduous broadleaf forests and MF displayed the most evident seasonal trend, with zero LUE at dormant winter season and highest LUE at summer growing months. Most of the DBF and MF sites (36 out of 42) were in the temperate (Köppen C group) or continental climate (Köppen D group) regions. Deciduous broadleaf forests and MF in temperate climate started photosynthesis earlier than those in continental climate; that is, photosynthesis started in April among 16 out of 17 temperate sites, while nine out of 19 continental sites started to sprout in May.

There were two major factors affecting grassland LUE. First, grassland photosynthesis in early spring behaved differently between the continental climate (Köppen D group) and temperate climate (Köppen C group), similar to patterns seen in DBF and MF. Temperate grassland sites started photosynthesis earlier than those in continental climate in early spring. This trend was especially evident for sites located at high

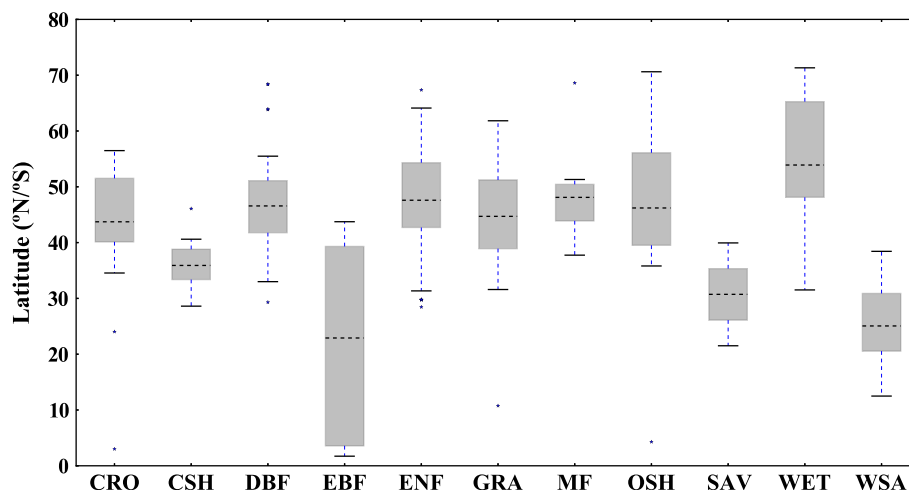


Fig. 6. Boxplot of latitude distribution of studied sites grouped by vegetation types (biomes). The median (horizontal blue dash lines), quartiles (boxes), and the 2.5th and 97.5th percentiles (vertical blue dash lines, indicating the 95% confidence interval) are marked. Most savannas (SAV), evergreen broadleaf forests (EBF), and woody savannas (WSA) sites are located at middle to low latitudes. \* indicates outliers.

latitudes. Second, grassland LUE values were sensitive to water stress during the summer months, which also had the highest light availability; the effects of water and light availabilities cancel out each other; therefore, grassland LUE had less conspicuous seasonality than other vegetation types.

#### *The role of climate data in predicting LUE*

The importance of biome classifications on LUE has been widely addressed, while the role of climate type and its interaction with seasonality on LUE has not been carefully scrutinized. To understand the contribution of different explanatory variables to the model performances, RFR models were run by removing one variable iteratively. Biome is the most important feature in determining LUE, followed by Köppen climate-type classifications (Appendix S1: Table S3). Since drought or water stress is apparently affecting the seasonal patterns of LUE significantly, this suggests that precipitation of the month might not be the best index as a measure of drought effects on GPP on a monthly basis.

The overall performance of predicting LUE using RFR with Kp was significantly higher than the simulation without Kp (Fig. 9 and Appendix S1: Table S2), especially in August. This poor performance without Kp in August was most

likely due to the vast difference between Mediterranean EBF and tropical EBF in their responses to environmental stress, especially by drought and warming stress (Tramontana et al. 2015). The most significant decline in  $r$  after removing Kp also occurred in early spring (February and March). In contrast, removing other meteorological variables (temperature and precipitation) actually slightly boosted  $r$  (Appendix S1: Table S3). This suggests that Kp is a much more reliable indicator of LUE in early spring than other meteorological variables such as temperature and radiation. Kp as one of the explanatory variables may improve model performance in two ways: First, it integrates detailed information of spring-time onset of photosynthesis of various ecosystems. Second, it enhances the predicting ability for EBF LUE, especially for summer months of the Northern Hemisphere. Our results suggest that Kp information is vital in determining phenological cycles of ecosystems and Kp is a strong indicator that integrates meteorological information in models of terrestrial carbon cycle.

#### *Covariance of GPP and climate variables*

Terrestrial carbon cycles are strongly entangled with climate drivers and carbon cycle–climate feedback dynamics and mechanisms are still unclear to researchers (Beer et al. 2010, Luo et al. 2015). In this research, we performed partial

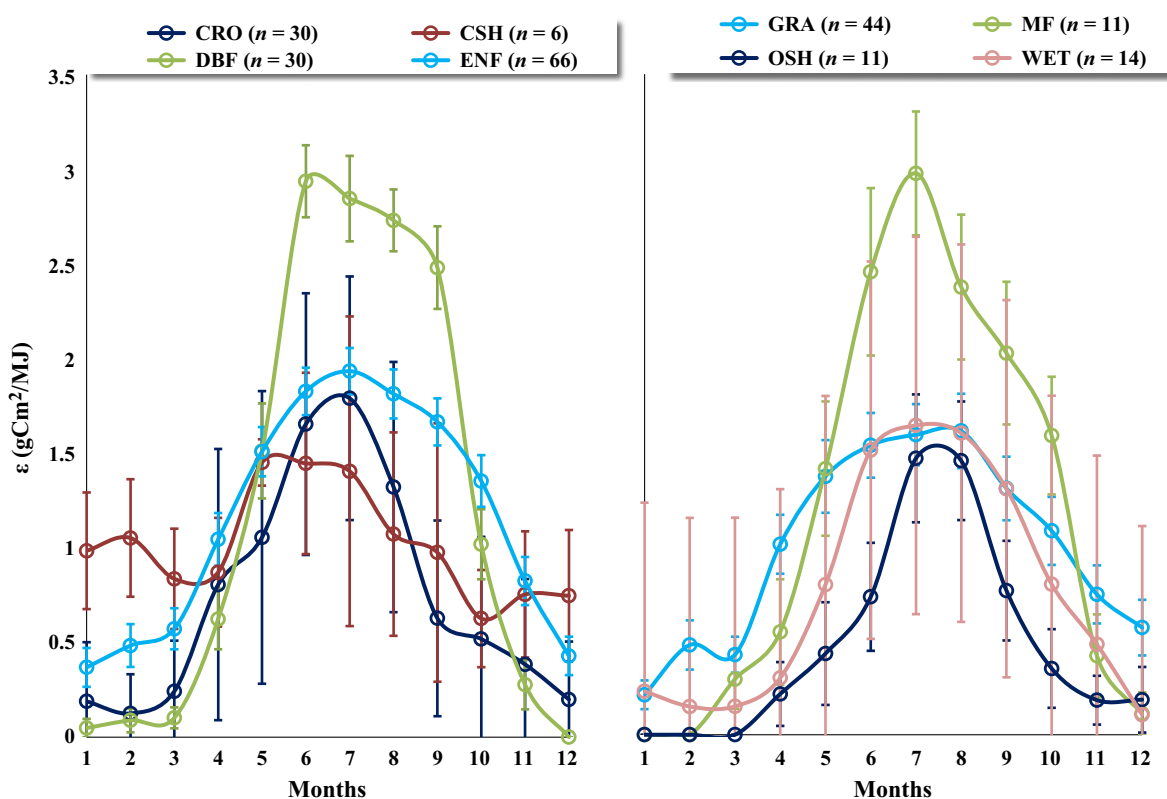


Fig. 7. Temporal variations in light-use efficiency and standard errors (defined as the standard deviation divided by the square root of number of sites) for biomes at middle to high latitude. Light-use efficiency was obtained by fitting a rectangular hyperbola model to the response of  $\text{CO}_2$  flux between the ecosystem and the atmosphere to absorbed photosynthetic flux density at monthly scale. Light-use efficiency was aggregated from site to biome level.

correlations of GPP estimated by RFR-LUE-GPP with temperature and precipitation. By controlling precipitation, we found robust positive correlations of GPP with temperature at middle to high latitudes as expected and negative correlations in most areas at middle to low latitudes (Fig. 10 top). By controlling temperature, we found a positive correlation of GPP ( $*P < 0.05$ ) with precipitation at central and southern Africa and central India (Fig. 10 bottom), suggesting that lack of moisture greatly restricted GPP in those regions. Although most subarctic climates have little precipitation, we also found some parts of subarctic region and also showed negative correlation between GPP and precipitation. It might be that extreme high precipitation could occur due to orographic effects. For instance, the negative correlation observed in the middle of

Labrador Island in eastern Canada may be associated with high precipitation due to the semi-permanent Icelandic low. That area can receive up to 1300 mm of rainfall equivalent per year, creating a snow cover that does not melt until June. Excess precipitation caused decreased GPP in this region.

## DISCUSSIONS

### *Threshold temperature for spring-time onset of photosynthesis is climate dependent*

Analysis with the RFR-LUE-GPP model suggested that including Köppen climate type greatly enhanced the model performance (Fig. 9 and Appendix S1: Table S2), suggesting that a general indicator of climate information is helpful for global carbon modeling. Our finding is also

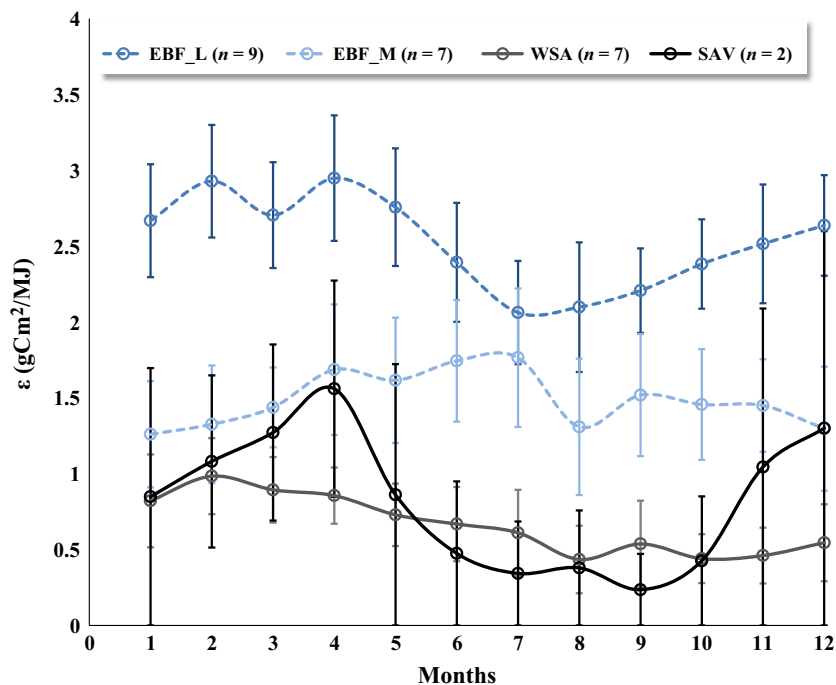


Fig. 8. Variations in light-use efficiency (LUE) and standard errors (defined as the standard deviation divided by the square root of number of sites) for biomes at middle to low latitudes. These three vegetation types tend to display little seasonal variations in LUE. There were two geographically distinct groups of evergreen broadleaf forests (EBF) sites. One group (EBF\_L) consisted of sites from tropical and the latitudes of these sites range from 15.4° S to 5.3° N. The other group (EBF\_M) was from mid-latitude European countries (Mediterranean climate) and Australia (oceanic climate). The latitudes range from 35.6° S to 37.4° S in Southern Hemisphere and from 38.5° N to 43.7° N in Northern Hemisphere. There was a significant difference between EBF\_M and EBF\_L LUE (Table 4,  $**P < 0.01$ ).

consistent with previous studies that demonstrated that the spring-time onset of photosynthesis in boreal forests is controlled by air and soil temperature and is particularly sensitive to snow depth in the dormant season and spring thaws (Tanja et al. 2003, Dunn et al. 2007), and it was suggested that these factors should be simulated in terrestrial biosphere models (Goulden et al. 1996, Dunn et al. 2007, Schaefer et al. 2012). However, modelers face great challenges in parameterizing the spring-time onset of photosynthesis when modeling the terrestrial carbon cycle at continental scale, which is so heterogeneous with respect to topography and climate. Usually, a minimum temperature required ( $T_{\min}$ ) for the spring-time onset of photosynthesis is applied as a model constraint. The MODIS GPP algorithm, for instance, used a  $T_{\min}$  of  $-8^{\circ}\text{C}$  (Running and Zhao 2015), below which cold temperatures shut

down photosynthesis. A higher  $T_{\min}$  at  $0^{\circ}\text{C}$  was applied as many studies found most LUE models over-predicted GPP at temperature below  $0^{\circ}\text{C}$ . Increasing the  $T_{\min}$  to  $0^{\circ}\text{C}$  for vegetation would reduce the positive bias in winter and spring in most LUE models (Schaefer et al. 2012, Yuan et al. 2014). Our results suggested that using a  $T_{\min}$  of  $0^{\circ}\text{C}$  is realistic when applied to vegetation under temperate climates (Köppen C group). However, this rule does not work when applied to vegetation in a continental climate (Köppen D group). For example, for the site CZ-BK2 (grasslands) in the Czech Republic, the monthly average temperature rebounded above zero (the actual temperature ( $T$ ) is greater than minimum required temperature, i.e.,  $T - T_{\min} > 0$ ) around late March and early April; however, photosynthesis started around late May, almost two months later. Similar patterns were found among boreal

Table 4. A two-factor ANOVA ( $\alpha = 0.05$ ) test was conducted on the latitudes and seasonality effects on EBF light-use efficiency.

Source	SS	df	MS	F	P-value	Significant
ML/LL	19.14	1	19.14	9.14	0.00**	Yes
Months	4.69	11	0.43	0.20	0.10	No
Interaction	6.08	11	0.55	0.26	0.99	No
Within	351.78	168	2.09			
Total	381.69	191	2.00			

Notes: EBF, evergreen broadleaf forests. LL means EBF sites from low latitudes (15.4° S–5.3° N,  $n = 7$ ), and ML means EBF from mid-latitudes (35.5° S–48.7° N,  $n = 7$ ). There was a significant difference between ML EBF and LL EBF (\*\* $P < 0.01$ ), while the monthly difference ( $P = 0.10$ ) and the interaction between latitudes and seasonality ( $P = 0.99$ ) were not significant.

vegetation with continental climate. For the CAN51 (evergreen needleleaf forests) site in Canada, minimum monthly winter temperature could be as low as  $-15^{\circ}\text{C}$  with the temperature rebounding above  $0^{\circ}\text{C}$  in April. Onset of photosynthesis at this site started in June with average monthly temperature above  $10^{\circ}\text{C}$ . Deciduous broadleaf forests and MF sites with early-onset photosynthesis were all within the temperate climate regions. Usually, thicker snow occurs with a

continental climate so that even though the air temperature rises above  $0^{\circ}\text{C}$ , it still takes weeks to melt all the snow and warm the roots. Consequently, climate information needs to be incorporated into modeling of the terrestrial carbon cycle.

### Deciphering the large uncertainties in predicting EBF GPP

For both mid-latitude EBF and tropical EBF, the LUE values from this study were significantly higher than those values used in most LUE models except for CFlux (Appendix S1: Table S4). The MODIS GPP algorithm used a constant of  $1.68 \text{ (g C}\cdot\text{m}^{-2}\cdot\text{MJ}^{-1} \text{ APAR)}$  for maximum LUE of EBF (Running et al. 2004, Yuan et al. 2014). This value was close to the LUE obtained from EBF sites under Mediterranean and temperate climates (located in mid-latitudes), but substantially lower than that from sites located in tropical regions, which indicated tropical EBF LUE was underestimated in those models.

Studies using machine-learning methods have shown that remote-sensing data representing greenness of a biome, such as EVI and  $f_{\text{PAR}}$ , were key drivers for accurate predictions of GPP with either high variability of greenness over the

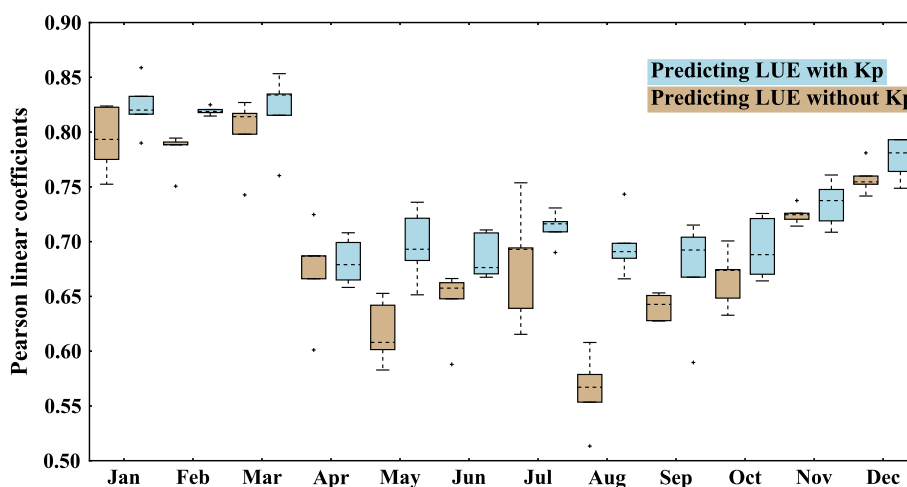


Fig. 9. Fivefold cross-validation coefficients (Pearson's linear coefficients)  $r$  between predicted light-use efficiency (LUE) by random forest regression (RFR) and LUE obtained from FLUXNET tower sites are presented above. We use Python scikit-learn module for the analysis (<http://scikit-learn.org/stable/modules/ensemble.html#forests-of-randomized-trees>). The blue color represents RFR modeling with Köppen climate-type classification (Kp) as one of explanatory variables. The tan color represents RFR modeling without Kp. Adding Köppen climate-type classification data improved model performance in August significantly (\*\* $P < 0.001$ , Appendix S1: Table S2). + indicates outliers.

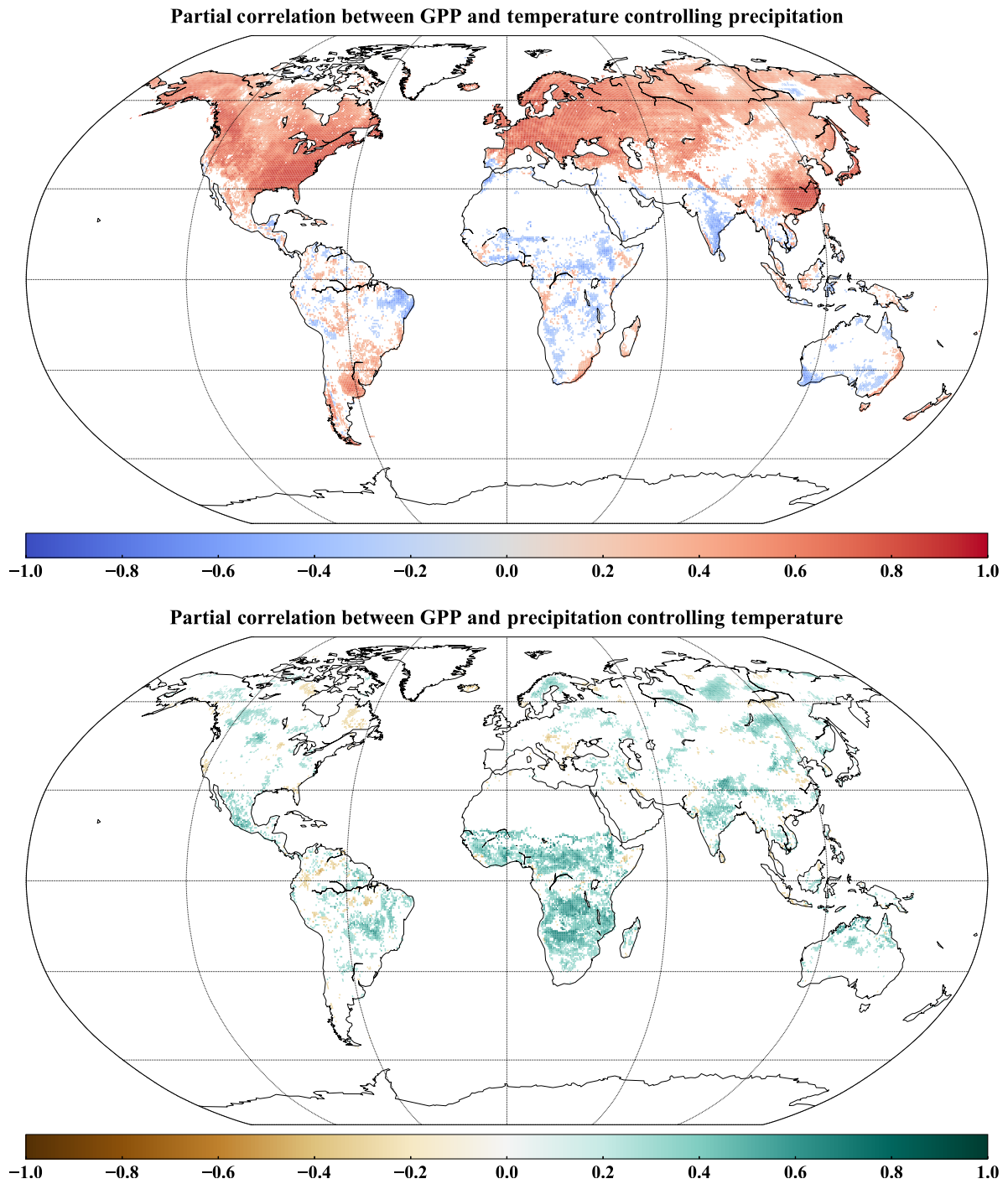


Fig. 10. Partial correlation between gross primary production (GPP) and temperature controlling precipitation (top) and partial correlation between GPP and precipitation controlling temperature (bottom). Blank areas indicate missing data, or linear correlation was not significant ( $P > 0.05$ ).

phenological cycle (e.g., DBF, MF) or that was highly affected by human management (e.g., croplands). In contrast, in ecosystems such as EBF with low variability of greenness, the model predictions were poor while using remote-sensing data. Instead, meteorological data may predict GPP with higher accuracy (Tramontana et al. 2015). Coincidentally, studies found LUE models underestimate DBF or MF GPP in summer (Schaefer et al. 2012) when plant canopies are fully developed and the LUE reaches levels similar to EBF LUE (Figs. 7, 8). Perhaps key environmental drivers such as water stress or nutrients need to be included in modeling.

The drought sensitivity of tropical forests is highly controversial (Saleska et al. 2007, Phillips et al. 2009, Tan et al. 2013). Two contrasting opinions exist. A study based on satellite images showed an Amazonian rainforest “green-up” during the severe drought of 2005 and suggested that tropical forests could be resilient to drought (Saleska et al. 2007). Phillips et al. (2009) believed the Amazonian forest was sensitive to drought; both decreased growth and increased mortality were observed in the forests during the 2005 drought. Da Costa et al. (2010) supported the position that tropical rainforests are sensitive to drought. Our results also supported the latter (Fig. 8). The decline of EBF\_L LUE from July to September was caused by drought stress of EBF sites under Aw climates during dry season (data not shown). The study by Goulden et al. (2004), which analyzed the net exchange of CO<sub>2</sub> between the atmosphere and an old-growth tropical forest in Para, Brazil, from July 2000 to July 2001, found “wood increment increased from January to May, suggesting greater rates of carbon sequestration during the wet season.” The paper also explained why the opposite opinion was often found in many studies: “However, the daily net CO<sub>2</sub> exchange measured by EC revealed the opposite trend, with greater carbon accumulation during the dry season. A reduction in respiration during the dry season was an important cause of this seasonal pattern.” Since our analysis was based on monthly time-step, a relative long-term trend in comparison with daily measurements, our finding was consistent with Goulden et al.’s (2004) results.

### *Disparity between LUE model vs. data-oriented model*

Light-use efficiency models usually involve complex combination of scientific assumptions. In contrast, data-driven models are contingent on availability and quality of sufficient explanatory data. With an increasing flow of data from the FLUXNET community and remote-sensing instruments, developments of better dialogical models are possible. Previous studies reported an estimate of global GPP ranged from 102 to 135 Pg C/yr and an average of 120 Pg C/yr with 95% confidence level from 1998 to 2005 (Beer et al. 2010). Estimates from data-oriented models consistently fell into an upper bin of 120–135 Pg C/yr, while estimates from LUE models always fell into a lower bin of 102–120 Pg C/yr. Although our results were consistent with the range:  $121.5 \pm 3.6$  Pg C/yr for RFR-GPP model and  $107.5 \pm 2.5$  Pg C/yr for RFR-LUE-GPP (Table 2), we suspect RFR-GPP algorithm had overestimated GPPs at certain regions of the world (Fig. 5). As shown in Fig. 5 and Table 2, the RFR-GPP model estimated much higher GPPs over sparsely vegetated areas at middle to low latitude (i.e., 10° S–40° S and 5° N–40° N), dominated by major vegetation types of SAV, WSA and OSH. There are much fewer towers located in these regions and towers are more likely to be located in well-vegetated areas than in average (or less than optimum) vegetation coverage, leading to skepticism about the machine-learning training results.

The area of SAV is largest among all the biomes but the estimation of SAV’s contribution to total GPP is highly controversial. The result from multi-model averaging reported by Beer et al. (2010) suggested that SAV contributed to 26% of global GPP and was ranked as the second most important biome. The highest estimate from our models was RFR-GPP at 9.5%. The estimates were even lower at 4.5% by the RFR-LUE-GPP (Table 2). This mismatch may come from uncertainties of land cover, or perhaps from less SAV data available for our calibrations (two sites included in this study). Although more FLUXNET sites have been established in recent years, those sites are clustered in Europe and northern America. To improve global GPP modeling capacity, more SAV sites are required especially at low latitudes.

## CONCLUSIONS

The effects of biome types, seasonality, and their interaction on LUE are highly significant for modeling global GPP. Biome LUE displayed evident seasonality at middle to high latitudes and less seasonality at low latitudes. Incorporating biome seasonality of LUE at monthly scale not only provides more accurate and comprehensive information for modeling purposes, but also provides insights on physiological mechanisms for plant phenology at biome scale with optimum temporal resolution.

Model performance can be significantly improved by adding Köppen climate classification data as an explanatory variable in the RFR approach, as it conveys the seasonal phenological state of the vegetation and improves the prediction of EBF GPP, especially in August. Also, Köppen climate type is a better indicator than temperature and precipitation in integrating meteorological information in terrestrial carbon cycle modeling.

Another line of evidence showing Köppen climate type is helpful for global carbon modeling lies in refining spring-time onset of photosynthesis condition. The threshold temperature for spring-time onset of photosynthesis updated by other studies at 0°C works well for biomes in temperate climate (Köppen C group), but not for continental climate (Köppen D group). The latter requires more energy for the spring thaw and to warm up the roots.

The RFR-GPP model tended to overestimate GPP in middle to low latitudes over sparsely vegetated areas (i.e., 10° S–40° S and 10° N–40° N) occupied by major vegetation types of SAV, WSA and OSH; more EC towers are required to reduce the modeling uncertainties.

The dominant climate drivers for global GPP generated by the RFR-LUE-GPP model are temperature at middle to high latitudes and water availability at low latitudes. The water stresses in low latitudes are expected to be enhanced by increased temperature and lack of precipitation as climate warming continues. These analyses echo the necessity of modeling the terrestrial carbon cycle and its feedback mechanisms by middle to low latitudes and middle to high latitudes separately.

## ACKNOWLEDGMENTS

This work used eddy covariance data acquired by the FLUXNET community and in particular by the following networks: AmeriFlux, FLUXNET-Canada, Carbon Europe IP, USCCC, China Flux, OZFLux, Carbon Africa, and Asia Flux networks. We thank all these data providers for making this high quality of measurements/products available to the scientific communities. The MODIS data used in this study are from the Land Processes Distributed Active Archive Center (LP DAAC), located at the U.S. Geological Survey (USGS) Earth Resources Observation and Science (EROS) Center (lpdaac.usgs.gov). We thank the data providers from the Institute for Environment and Sustainability (IES) at the Joint Research Center of the European Commission. We acknowledge the researchers and scientists from National Centers for Environmental Prediction (NCEP) reanalysis program for providing climate data. Especially, we want to thank Dr. Peel from The University of Melbourne, Australia, for making Köppen climate classification data available to the public. This data processing was completed at the Center for Computational Infrastructure for the Sciences (CCIS) at Queens College. This research was supported by PSC-CUNY CIRG-80209-08 22.

## LITERATURE CITED

- Aubinet, M. 2008. Eddy covariance CO<sub>2</sub> flux measurements in nocturnal conditions: an analysis of the problem. *Ecological Applications* 18:1368–1378.
- Aubinet, M., B. Heinesch, and M. Yernaux. 2003. Horizontal and vertical CO<sub>2</sub> advection in a sloping forest. *Boundary Layer Meteorology* 108:397–417.
- Baldocchi, D. 2008. 'Breathing' of the terrestrial biosphere: lessons learned from a global network of carbon dioxide flux measurement systems. *Australian Journal of Botany* 56:1–26.
- Baldocchi, D., et al. 2001. FLUXNET: a new tool to study the temporal and spatial variability of ecosystem-scale carbon dioxide, water vapor and energy flux densities. *Bulletin of the American Meteorological Society* 82:2415–2434.
- Barton, C. V. M., and P. R. J. North. 2001. Remote sensing of canopy light use efficiency using the photochemical reflectance index: model and sensitivity analysis. *Remote Sensing of Environment* 78: 264–273.
- Beer, C., et al. 2010. Terrestrial gross carbon dioxide uptake: global distribution and covariation with climate. *Science* 329:834–838.
- Chen, M., P. Xie, and J. E. Janowiak. 2002. Global land precipitation: a 50-yr monthly analysis based on

- gauge observations. *Journal of Hydrometeorology* 3:249–266.
- Cox, P. M., R. A. Betts, C. D. Jones, S. A. Spall, and I. J. Totterdell. 2000. Acceleration of global warming due to carbon-cycle feedbacks in a coupled climate model. *Nature* 408:184–187.
- Cox, P. M., D. Pearson, B. B. Booth, P. Friedlingstein, C. Huntingford, C. D. Jones, and C. M. Luke. 2013. Sensitivity of tropical carbon to climate change constrained by carbon dioxide variability. *Nature* 494:341–344.
- Da Costa, A. C., et al. 2010. Effect of 7 yr of experimental drought on vegetation dynamics and biomass storage of an eastern Amazonian rainforest. *New Phytologist* 187:579–591.
- Dunn, A., C. C. Barford, S. C. Wofsy, M. L. Goulden, and B. C. Daube. 2007. A long-term record of carbon exchange in a boreal black spruce forest: means, responses to inter-annual variability, and decadal trends. *Global Change Biology* 13:577–590.
- Falge, E., et al. 2001. Gap filling strategies for defensible annual sums of new ecosystem exchange. *Agricultural and Forest Meteorology* 107:43–69.
- Farquhar, G. D., S. Caemmerer, and J. A. Berry. 1980. A biochemical model of photosynthetic CO<sub>2</sub> assimilation in leaves of C3 species. *Planta* 149: 78–90.
- Feigenwinter, C., C. Bernhofer, and R. Vogt. 2005. The influence of advection on short-term CO<sub>2</sub> budget in and above a forest canopy. *Boundary Layer Meteorology* 113:201–224.
- Feigenwinter, C., M. Mölder, A. Lindroth, and M. Aubinet. 2010a. Spatiotemporal evolution of CO<sub>2</sub> concentration, temperature, and wind field during stable nights at Norunda forest site. *Agricultural Forest Meteorology* 150:692–701.
- Feigenwinter, C., L. Montagnani, and M. Aubinet. 2010b. Plot-scale vertical and horizontal transport of CO<sub>2</sub> modified by a persistent slope wind system in and above an alpine forest. *Agricultural Forest Meteorology* 150:665–673.
- Feigenwinter, C., et al. 2008. Comparison of horizontal and vertical advective CO<sub>2</sub> fluxes at three forests sites. *Agricultural Forest Meteorology* 149:12–14.
- Field, C. B. 1991. Ecological scaling of carbon gain to stress and resource availability. Pages 35–65 in H. A. Mooney, S. E. Winner, and E. J. Pell, editors. *Integrated responses of plants to stress*. Academic Press, San Diego, California, USA.
- Finnigan, J. 2008. An introduction to flux measurements in difficult conditions. *Ecological Applications* 18:1340–1350.
- Gobron, N. B., et al. 2006. Evaluation of fraction of absorbed photosynthetically active radiation products for different canopy radiation transfer regions: methodology and results using Joint Research Center products derived from SeaWiFS against ground-based estimations. *Journal of Geophysical Research* 111:D13110.
- Goetz, S. J., S. D. Prince, S. N. Goward, M. M. Thawley, and J. Small. 1999. Satellite remote sensing of primary production: an improved production efficiency modeling approach. *Ecological Modeling* 122:239–255.
- Goulden, M. L., S. D. Miller, H. R. Da Rocha, M. C. Mento, H. C. De Freitas, A. M. S. Figueira, and C. A. D. De Sousa. 2004. Diel and seasonal patterns of tropical forest CO<sub>2</sub> exchange. *Ecological Applications* 14(Suppl 4):42–54.
- Goulden, M. L., J. W. Munger, S. M. Fan, C. D. Bruce, and S. C. Wofsy. 1996. Exchange of carbon dioxide by a deciduous forest: response to internal climate variability. *Science* 271:1575–1578.
- Hilker, T., N. C. Coops, M. A. Wulder, T. A. Black, and R. D. Guy. 2008. The use of remote sensing in light use efficiency based models of gross primary production: a review of current status and future requirements. *Science of the Total Environment* 404:411–423.
- Jung, M., M. Reichstein, and A. Bondeau. 2009. Towards global empirical upscaling of FLUXNET eddy covariance observations: validation of a model tree ensemble approach using a biosphere model. *Biogeosciences* 6:2001–2013.
- Jung, M., et al. 2011. Global patterns of land atmosphere fluxes of carbon dioxide, latent heat, and sensible heat derived from eddy covariance, satellite, and meteorological observations. *Journal of Geophysical Research* 116:G00J07.
- Lambers, H., F. S. S. Chapin III, and T. L. Pons. 1998. *Plant physiological ecology*. Pages 230–238 in *Scaling-up gas exchange and energy balance from the leaf to the canopy level*. Springer-Verlag, New York, New York, USA.
- Luo, Y., T. F. Keenan, and M. Smith. 2015. Predictability of the terrestrial carbon cycle. *Global Change Biology* 21:1737–1751.
- Massman, W. J., and X. Lee. 2002. Eddy covariance flux corrections and uncertainties in long-term studies of carbon and energy exchange. *Agricultural and Forest Meteorology* 113:121–144.
- Medlyn, B. E. 1998. Physiological basis of the light use efficiency model. *Tree Physiology* 18:167–176.
- Montagnani, L., et al. 2009. A new mass conservation approach to the study of CO<sub>2</sub> advection in an alpine forest. *Journal of Geophysical Research* 114: D07306.
- Monteith, J. L. 1972. Solar radiation and productivity in tropical ecosystems. *Journal of Applied Ecology* 9:747–766.

- Papale, D., and R. Valentini. 2003. A new assessment of European forests carbon exchanges by eddy fluxes and artificial neural network spatialization. *Global Change Biology* 9:525–535.
- Papale, D., et al. 2006. Towards a standardized processing of Net Ecosystem Exchange measured with eddy covariance technique: algorithms and uncertainty estimation. *Biogeosciences* 3:571–583.
- Pedregosa, F., et al. 2011. Scikit-learn: machine learning in Python. *Journal of Machine Learning Research* 12:2825–2830.
- Peel, M. C., B. L. Finlayson, and T. A. McMahon. 2007. Updated world map of the Köppen climate classification. *Hydrology and Earth System Sciences Discussions European Geosciences Union* 11: 1633–1644.
- Phillips, O. L., et al. 2009. Drought sensitivity of the Amazon rainforest. *Science* 323:1344–1347.
- Prince, S. D. 1991. A model of regional primary production for use with coarse resolution satellite data. *International Journal of Remote Sensing* 12:1313–1330.
- Raczka, B. M., et al. 2013. Evaluation of continental carbon cycle simulations with North American flux tower observations. *Ecological Monographs* 83: 531–556.
- Reichstein, M., et al. 2005. On the separation of net ecosystem exchange into assimilation and ecosystem respiration: review and improved algorithm. *Global Change Biology* 11:1424–1439.
- Ruimy, A., P. G. Jarvis, D. D. Baldocchi, and B. Saugier. 1995. CO<sub>2</sub> fluxes over plant canopies and solar radiation: a review. *Advances in Ecological Research* 26:1–68.
- Running, S. W., R. R. Nemani, F. A. Heinsch, M. Zhao, M. Reeves, and H. Hashimoto. 2004. A continuous satellite-derived measure of global terrestrial primary production. *Biogeoscience* 54:547–560.
- Running, S. W., and M. Zhao. 2015. User's guide: GPP and NPP (MOD17A2/A3) products. NASA MODIS land algorithm, version 3.0. [http://www.ntsg.umt.edu/sites/ntsg.umt.edu/files/modis/MOD17UsersGuide2015\\_v3.pdf](http://www.ntsg.umt.edu/sites/ntsg.umt.edu/files/modis/MOD17UsersGuide2015_v3.pdf)
- Saleska, S. R., K. Didan, A. R. Huete, and H. R. Da Rocha. 2007. Amazon forests green-up during 2005 drought. *Science* 318:612.
- Schaefer, K., et al. 2012. A model-data comparison of gross primary productivity: results from the North American Carbon Program site synthesis. *Journal of Geophysical Research* 117:G03010.
- Sellers, P. J., S. O. Los, C. J. Tucker, C. O. Justice, D. A. Dazlich, G. J. Collatz, and D. A. Randall. 1996. A revised land surface parameterization (SiB2) for atmospheric GCMs. Part II: the generation of global fields of terrestrial biophysical parameters from satellite data. *Journal of Climate* 9:706–737.
- Tan, Z. H., M. Cao, G. R. Yu, J. W. Tang, X. B. Deng, Q. H. Song, and Y. Deng. 2013. High sensitivity of a tropical rainforest to water variability: evidence from 10 years of inventory and eddy flux data. *Journal of Geophysical Research: Atmospheres* 118:9393–9400.
- Tanja, S., et al. 2003. Air temperature triggers the recovery of evergreen boreal forest photosynthesis in spring. *Global Change biology* 9:1410–1426.
- Tramontana, G., K. Ichii, G. Camps-Valls, E. Tomelleri, and D. Papale. 2015. Uncertainty analysis of gross primary production upscaling using Random Forests, remote sensing and eddy covariance data. *Remote Sensing of Environment* 168:360–373.
- Turner, D. P., W. D. Ritts, W. B. Cohen, S. T. Gower, M. Zhao, S. W. Running, S. C. Wofsy, S. Urbanski, A. L. Dunn, and J. W. Munger. 2003a. Scaling gross primary production (GPP) over boreal and deciduous forest landscapes in support of MODIS GPP product validation. *Remote Sensing of Environment* 88:256–270.
- Turner, D. P., S. Urbanski, D. Bremer, S. C. Wofsy, T. Meyers, S. T. Gower, and M. Gregory. 2003b. A cross-biome comparison of light use efficiency for gross primary production. *Global Change Biology* 9:383–395.
- Vetter, M., et al. 2008. Analyzing the causes and spatial pattern of the European 2003 carbon flux anomaly using seven models. *Biogeosciences* 5: 561–583.
- Wei, S., et al. 2014. Data-based perfect-deficit approach to understanding climate extremes and forest carbon assimilation capacity. *Environment Research Letter* 9:065002.
- Xiao, X. 2006. Light absorption by leaf chlorophyll and maximum light use efficiency. *IEEE Transactions on Geoscience and Remote Sensing* 44:1933–1935.
- Xiao, J., et al. 2014. Data-driven diagnostics of terrestrial carbon dynamics over North America. *Agricultural and Forest Meteorology* 197:157.
- Yang, F., K. Ichii, M. A. White, H. Hashimoto, A. R. Michaelis, P. Votava, A. X. Zhu, A. Huete, S. W. Running, and R. R. Nemani. 2007. Developing a continental-scale measure of gross primary production by combining MODIS and AmeriFlux data through Support Vector Machine approach. *Remote Sensing of Environment* 110:109–122.
- Yi, C., D. E. Anderson, A. A. Turnipseed, S. P. Burns, J. P. Sparks, D. I. Stannard, and R. K. Monson. 2008. The contribution of advective fluxes to net ecosystem exchange in a high-elevation, subalpine forest. *Ecological Applications* 18:1379–1390.

- Yi, C., K. J. Davis, P. S. Bakwin, B. W. Berger, and L. Marr. 2000. The influence of advection on measurements of the net ecosystem-atmosphere exchange of CO<sub>2</sub> from a very tall tower. *Journal of Geophysical Research* 105:9991–9999.
- Yi, C., E. Pendall, and P. Ciais. 2015. Focus on extreme events and the carbon cycle. *Environmental Research Letters* 10:070201.
- Yi, C., S. Wei, and G. Hendrey. 2014. Warming climate extends dryness-controlled areas of terrestrial carbon sequestration. *Scientific Reports*. <https://doi.org/10.1038/srep05472>
- Yi, C., et al. 2004. A nonparametric method for separating photosynthesis and respiration components in CO<sub>2</sub> flux measurements. *Geophysical Research Letters* 31:L17107. <https://doi.org/10.1029/2004GL020490>
- Yuan, W., et al. 2014. Vegetation-specific model parameters are not required for estimating gross primary production. *Ecological Modeling* 292:1–10.
- Zhao, M., F. A. Heinsch, R. R. Nemani, and S. W. Running. 2005. Improvements of the MODIS terrestrial gross and net primary production global data set. *Remote Sensing of Environment* 95: 164–176.
- Zhao, M., and S. W. Running. 2006. Sensitivity of Moderate Resolution Imaging Spectroradiometer (MODIS) terrestrial primary production to the accuracy of meteorological reanalysis. *Journal of Geophysical Research* 111:G01002.

### SUPPORTING INFORMATION

Additional Supporting Information may be found online at: <http://onlinelibrary.wiley.com/doi/10.1002/ecs2.1724/full>